Nagra, M., Gilmartin, B., Thai, N. J., & Logan, N. S. (2017). Determination of retinal surface area. *Journal of Anatomy*, *231*(3), 319-324. https://doi.org/10.1111/joa.12641

TITLE: Determination of retinal surface area

Running title: Retinal surface area

AUTHOR DETAILS AND INSTITUTIONAL AFFILIATIONS:

Manbir Nagra[1], Bernard Gilmartin[2], Ngoc Jade Thai[3], Nicola S. Logan[2]

[1]Applied Vision Research Centre, Division of Optometry and Visual Science, City, University of London, EC1V 0HB, United Kingdom

[2]School of Life and Health Sciences, Aston University, Birmingham, B4 7ET, United Kingdom

[3]Clinical Research & Imaging Centre, University of Bristol, Bristol, BS2 8DX, United Kingdom

Corresponding Author: Manbir Nagra

Email address: Manbir.Nagra.1@city.ac.uk

Postal address: Division of Optometry and Visual Science, City, University of London, EC1V 0HB, United Kingdom

ABSTRACT

Previous attempts at determining retinal surface area and surface area of the whole eye have been derived from mathematical calculations based upon retinal photographs, schematic eyes and from retinal biopsies of donor eyes. 3-D ocular magnetic resonance imaging (MRI) allows a more direct measurement, it can be used to image the eye *in vivo*, and there is no risk of tissue shrinkage. The primary purpose of this study is to compare, using T2-weighted 3-D MRI, retinal surface areas for superior-temporal (ST), inferior-temporal (IT), superior-nasal (SN) and inferior-nasal (IN) retinal quadrants. An ancillary aim is to examine whether inter-quadrant variations in area are concordant with reported inter-quadrant patterns of susceptibility to retinal breaks associated with posterior vitreous detachment (PVD).

Seventy-three adult participants presenting without retinal pathology (mean age 26.25±6.06 years) were scanned using a Siemens 3-Tesla MRI scanner to provide T2-weighted MR images that demarcate fluid-filled internal structures for the whole eye and provide high-contrast delineation of the vitreous-retina interface. Integrated MRI software generated total internal ocular surface area (TSA). The second nodal point was used to demarcate the origin of the peripheral retina in order to calculate total retinal surface area (RSA) and quadrant retinal surface areas (QRSA) for ST, IT, SN, and IN quadrants. Mean Spherical Error (MSE) was -2.50±4.03D and mean axial length (AL) 24.51±1.57mm. Mean TSA and RSA for the RE were 2058±189mm^2 and 1363±160mm^2, respectively. Repeated measures ANOVA for QRSA data indicated a significant difference within-quadrants ($p<0.01$) which, contrasted with ST (365±43mm^2), was significant for IT (340±40mm^2 $p<0.01$), SN (337±40mm^2 $p<0.01$) and IN (321±39mm^2 $p<0.01$) quadrants. For all quadrants QRSA was significantly correlated with AL ($p<0.01$) and exhibited equivalent increases in retinal area/mm increase in AL. Although the differences between QRSAs are relatively small, there was evidence of concordance with reported inter-quadrant patterns of susceptibility to retinal breaks associated with PVD. The data allow AL to be converted to QRSAs, which will assist further work on inter-quadrant structural variation.

Keywords: Ocular Biometry, Ocular Shape, Myopia, Retinal surface area, Human ocular anatomy

Introduction

Earlier attempts at determining retinal surface area and surface area of the whole eye have been derived from mathematical calculations based upon retinal photographs (Lempert, 2008; Croft et al. 2014), schematic eyes (Taylor and Jennings, 1971) and from retinal biopsies of donor eyes (Robb 1982; Panda-Jonas et al. 1994) (see Table 1). MRI possesses several advantages over previous methods used to quantify retinal surface area: unlike donor eye dissection, MRI is carried out *in vivo*, hence there is no risk of tissue shrinkage; additionally, MRI allows a more direct measurement and does not rely upon approximate schematic eye models. We have reported previously on the use of T2-weighted 3-dimensional (3-D) MRI to measure *in vivo* ocular volume and shape of the posterior vitreous chamber (Nagra et al. 2014; Gilmartin et al. 2013). As the technique is based on high-contrast delineation of the vitreo-retinal interface it can also be used to determine internal surface area of the retina.

Although 3-D MRI has been used previously to determine surface area in Singaporean-Chinese newborn and young children's eyes it has been restricted to total ocular surface area (TSA) (Lim et al. 2013; Lim et al 2011). In addition to determining TSA we use T2-weighted 3-D MRI to compare total retinal surface area (RSA) and retinal surface areas separately for superior-temporal (ST), inferior-temporal (IT), superior-nasal (SN) and inferior-nasal (IN) retinal quadrants. (QRSA). Although adults without presenting pathology are used in the present study (and with the presumption that there is a correlation between RSA and propensity to retinal anomalies) the ability to measure separately RSA for different retinal quadrants is an opportunity to examine two recent studies on eyes with rhegmatogenous retinal detachment (RRD). In their observational single-centre case series, Shunmugam et al. (2014) analysed 844 patients with a mean age of 62±11 years. Retinal breaks occurred most frequently in the ST quadrant (582 eyes; 69%); the superonasal and inferotemporal quadrants were involved in 341 (40%) and 274 (32%) eyes, respectively; the IN quadrant was involved the least frequently (144 eyes; 17%). Of the 328 eyes with only 1 break, it was most likely to be in the ST quadrant (182 eyes; 55%) and least likely to be in the IN quadrant (19 eyes; 6%). It was observed that quadrant breaks subsequent to an initial ST

break would follow the sequence of SN, IT, and then IN. Further, the proportion of breaks that were detached was highest for the ST quadrant (92%) and lowest for the IN quadrant (60%) a feature that was linked to the proposal that posterior vitreous detachment (PVD) follows a sequential process starting in the ST quadrant and progressing inferiorly or, alternatively, to be the result of gravitational force.

Similar findings were reported by Mitry et al. (2011), who found the percentage of RRD cases associated with PVD and related tractional tears was 86.3% and distributed as follows: 56% in the ST quadrant; 25.7% in the SN quadrant; 13.2% in the IT quadrant; 5.0% in the IN quadrant.

The primary purpose of the study is to use T2-weighted 3-D MRI to compare retinal surface areas TSA, RSA and QRSAs in adult eyes for a wide range of longitudinal axial lengths and hence refractive error. An ancillary aim is to examine whether inter-quadrant variations in area are concordant with reported inter-quadrant patterns of susceptibility to retinal breaks associated with posterior vitreous detachment (PVD).

METHODS

The study was approved by the Aston University Ethics Committee; all aspects of the investigation were carried out in accordance with the tenets of the Declaration of Helsinki. Informed consent was obtained from all individual participants included in the study.

Participants

Seventy-three adult participants, presenting without retinal pathology, were mainly recruited from a university student and staff population (females n=47, males n=26). Participant age ranged from 18 to 40 years (mean 26±6) and participants were predominantly of white European (n=56%) and South Asian (n=38%) ethnicity. Right eye data are presented.

Refractive Error and Axial Length

Objective measurements of refractive error were obtained under cycloplegia (one drop, in each eye, of tropicamide ophthalmic solution 0.5%, *Minims*® Bausch and Lomb, Surrey U.K) using the Shin Nippon SRW-5000 open-view binocular infrared autorefractor (Ryusyo Industrial Co. Ltd, Osaka, Japan). Five measurements of refractive error were taken from each eye, averaged, and expressed as mean spherical error (MSE, D). The Zeiss *IOLMaster* (Carl Zeiss Meditec, Germany) was used to measure both axial length (AL) and anterior chamber depth (ACD). The instrument's measurement principles for AL are based on partial coherence interferometry (PCI), and based on an optical section to determine ACD from the anterior cornea to the anterior crystalline lens. AL (mm) was expressed as the mean of five measurements and a single capture automatically generated mean ACD (mm) based on five measurements.

Acquisition of MR images and surface areas

The protocol, verification, and repeatability statistics for the MRI technique employed in this study have been previously reported, including the method used to locate the visual axis (Nagra et al. 2014; Gilmartin et al. 2013; Singh et al. 2006); the technique has been applied previously to the measurement of internal ocular volume and ocular shape (Nagra et al. 2014; Gilmartin et al. 2013).

In summary, participants underwent scanning using a Siemens Trio 3-Tesla whole-body MRI scanner using an 8-channel Phased-Array head-coil (Nagra et al. 2014; Gilmartin et al. 2013; Singh et al. 2006). A T2-weighted scan was used to demarcate fluid-based intraocular structures for each eye and thus provide high-contrast delineation of the internal surface of the eye including the vitreous-retina interface. The scan used a Half-Fourier Acquired Single-shot Turbo spin Echo (HASTE) sequence with parameters that provided isotropic voxel dimensions of 1x1x1mm. The scan time for each participant was 5 minutes 40 seconds, during which participants were asked to fixate steadily, with minimal blinking where possible, a distant fixation light viewed through a mirror mounted on the head-coil. Cycloplegia was not induced for the MRI scans.

Voxels were labelled using a 3-D flood-filling algorithm and automatically shaded. Axial, sagittal and coronal slices (between 22 and 29 slices per plane depending on globe dimensions) were then inspected and edited manually (by author MN) to rectify errors in automatic shading.

A shrink-wrapping process followed the shading procedure whereby a model of a sphere is first constructed using a mesh of 32768 triangular polygons of equal area distributed uniformly across its surface and the vertices of each polygon shrunk towards the geometric centre of the eye in an iterative fashion until each vertex intersects a shaded voxel. The process alters the position of the vertices of each polygon that results in the redistribution and resizing of polygons across an initial internal representation of the eye globe.

The corrugated shell generated is then smoothed, using local averaging of the vertex positions, to produce an internal interface. The surface model is defined by a standardised x-y-z 3-D coordinate system for each of the 32768 triangular polygons.

Total internal surface area of the globe (TSA) was provided by customised freeware software mri3dX and compared with the surface area of an equivalent sphere based on participants' longitudinal axial lengths using the standard formula for surface area (i.e. area=$4\pi r^2$ where r = PCI axial length/2, see Table 3 and Figure 2) (see references Singh et al. 2006, Gilmartin et al. 2013, Nagra et al. 2014 for additional detail).

The mri3dx software (Gilmartin et al. 2013; Singh et al. 2006) also provided, separately for each quadrant, areas of spherical segments that were contiguous with 1% linear increments along the visual axis. The location of the second nodal point (NP2) was assigned to the intersection of the posterior pole of the crystalline lens with the visual axis such that the line passing through NP2 and orthogonal to the axis demarcates approximately the origin of the peripheral retina. The approximate location of NP2 was determined from measurement of the ACD and an assumed average lens thickness of 3.75mm based on 3D MRI lens data from a similar participant group (Sheppard et al. 2011). Total retinal surface area and retinal surface area for each quadrant (QRSAs: ST, SN, IT, IN) was then determined by the successive summation of each 1% increment of surface area from a point corresponding to NP2 to a point 95% along the visual axis (Gilmartin et al. 2013). Consistent with our previous report (Gilmartin et al. 2013), retinal areas were not sampled for the posterior 5% of longitudinal axial length owing to motion artefacts as the value of x (the height of the spherical sector from the visual axis) approached an asymptote as the maximum value

of y (distance along the visual axis) was approached). With reference to a sphere of diameter equal to the mean AL of the group (24.51mm) the spherical cap forming the posterior 5% region represented only 4.55% of total internal eye area [(93.60/2057.65*100) mm^2].

Statistical Analyses

Statistical analyses were conducted using IBM SPSS Statistics 21 (IBM UK Ltd Portsmouth, UK). The level of statistical significance was taken as 5%. A repeated measures ANOVA was used to test differences between the four quadrants and planned contrasts were used to test, against quadrant ST, differences in mean retinal area for quadrants IT, SN and IN.

RESULTS

Paired Student's t-test showed no significant inter-eye differences for Mean Spherical Error (MSE) ($p=0.12$) or axial length ($p=0.88$); right eye data only are presented. As anticipated a more myopic MSE was correlated with a longer PCI AL ($p<0.01$, $r=0.88$).

Mean group data for MSE, AL, TSA and QRSAs are shown in Table 2. A one-way ANOVA, with gender as the between-subject factor, showed female participants to have a significantly more myopic mean MSE ($p=0.006$), but there were no significant differences between males and females in TSA, QRSAs or AL (all $p>0.05$).

Total Internal Surface Area (TSA)

Mean TSA was 2058±189mm^2. Scatter plots indicated an increase in TSA as refractive error increased towards myopia (Figure 1 A), and with increasing axial length (Figure 1 B).

To compare TSA generated by MRI with the TSA for an equivalent sphere, based solely on a measure of AL, the surface area of a sphere was calculated for each participant using the standard formula for surface area=$4\pi r^2$, where r = PCI axial length/2. Scatter plots of the two surface area estimates against axial length (Figure 2 and Table 3) demonstrated an underestimation of TSA using the sphere formula of 289mm^2 for axial lengths of 22mm and an overestimation of 34mm^2 for axial lengths of 28mm with parity at approximately 27.50mm.

Surface area of the retina

Total Retinal Surface Area (RSA)

Mean total RSA (i.e. all quadrants combined) was 1363±160mm^2 and showed significant correlations with PCI AL ($p<0.01$, $r=0.85$) and MSE ($p<0.01$, $r=-0.75$) (see Figure 1 C&D).

Quadrant Retinal Surface Areas (QRSAs)

QRSAs were largest for the ST quadrant and smallest for the IN quadrant. A repeated measures ANOVA for QRSA data indicated significant differences within- quadrants ($p<0.01$). Planned contrasts against the ST quadrant (365±43mm^2) were all significant : IT (340±40 mm^2 $p<0.01$), SN (337±40 mm^2 $p<0.01$) and IN (321±39mm^2 $p<0.01$)

DISCUSSION

We believe this to be the first study to measure *in vivo*, using MRI, total internal surface area (TSA), retinal surface area (RSA) and quadrant retinal surface areas (QRSAs) in human adult eyes (see Table 1).

As anticipated, we observe significant positive correlations between greater surface area, longer axial length, and increase in myopic refractive error (Figures 1 & 3). The data indicate that, similar to our findings on total ocular volume (Nagra et al. 2014), accurate estimates of TSA cannot be made from the application of a spherical model based simply on longitudinal axial length, particularly with regard to shorter axial lengths (Figure 2 and Table 3). The second-order polynomial fits in Figure 3 allow longitudinal axial lengths to be converted to retinal surface areas for each respective quadrant. For example, ST retinal surface areas for an axial length of 23.65mm (typical for an emmetropic eye) are 346mm^2, for 25mm 375mm^2, for 26.5mm 413mm^2 and for 28mm 455mm^2. Relative to the emmetropic eye these values of axial length represent percentage increases of 8.38%, 19.36% and 31.50% respectively. Using the formula for retinal surface area (Fig 2), we find our data compare well with Taylor and Jennings' prediction based on schematic eyes (see Table 1); a difference in area of 35mm^2 for an axial length of 22.12 mm.

That sphericity is a feature of the myopic eye was reported in the studies on ocular volume (Nagra et al. 2014) and ocular shape (Gilmartin et al. 2013) and is again clearly evident from Figure 2: TSA approaches that generated by an equivalent sphere as axial length, and hence myopic error, increases. With reference to our data on mean quadrant retinal surface areas (QRSAs), relative to the ST quadrant there was general concordance between the sequence of percentage ratios found (ST:1.0; SN:0.92; IT: 0.93; IN:0.88; Table 2) and the sequence of retinal breaks (expressed as percentage ratios for prevalence) reported by Shunmugam et al. (2014) (ST:1.0; SN:0.58; IT: 0.46; IN:0.25) and Mitry et al. (2011) (ST:1.0; SN:0.46; IT:0.24; IN:0.09) although the level of differentiation between quadrants was substantially less. Nevertheless mean retinal surface area of the ST quadrant was significantly greater than that of the IN quadrant by 12%, a difference which may, at least in part, contribute to additional biomechanical stress on retinal tissue in the ST quadrant and a hence a propensity to retinal breaks.

Of interest is that the relative difference between ST and IN quadrants is independent of axial length (Figure 3) and hence brings into question whether susceptibility to retinal breaks is determined by the inter-quadrant differentials of retinal surface area rather than the absolute levels of surface area . Neither Shunmugam et al. (2014) nor Mitry et al. (2011) carried out a detailed analysis of their data with reference to axial length and the literature on the correlation between axial length and retinal breaks is equivocal (Shunmugam et al. 2014; Mitry et al. 2011; Ogawa and Tanaka 1987; Pierro et al. 1992; Cheng et al. 2013).

Declaration of interest: The authors report no conflicts of interest. The authors alone are responsible for the content and writing of the paper

Acknowledgments: We acknowledge Krish D Singh, Elizabeth Wilkinson, Jon Wood for assistance with the MRI data collection, Robert P Cubbidge for assistance with data analysis, Catherine Suttle and John Lawrenson for their comments on earlier versions of the manuscript.

Disclosure of funding sources: College of Optometrists UK, the Lord Dowding Fund for Humane Research, Advantage West Midlands.

References

Lempert P. Optic disc area and retinal area in amblyopia. Seminars in Ophthalmology 2008; 23:302-306.

Croft DE, Van Hemert J, Wykoff CC, Clifton D, Verhoek M, Fleming A, & Brown DM. Precise montaging and metric quantification of retinal surface area from ultra-widefield fundus photography and fluorescein angiography. Ophthal Surg Las Im 2014; 45:312-317.

Taylor E, Jennings A. Calculation of total retinal area. Br J Ophthalmol 1971; 55:262-265.

Robb, RM. Increase in retinal surface area during infancy and childhood. Journal of pediatric ophthalmology and strabismus 1982; 19.4:16-20.

Panda-Jonas S, Jonas JB, Jakobczyk M & Schneider U. Retinal photoreceptor count, retinal surface area, and optic disc size in normal human eyes. Ophthalmology 1994; 101:519-523.

Nagra M, Gilmartin B, Logan NS. Estimation of ocular volume from axial length. Br J Ophthalmol 2014;98:1697-1701.

Gilmartin B, Nagra M, Logan NS. Shape of the posterior vitreous chamber in human emmetropia and myopia. Invest Ophthalmol Vis Sci 2013;54:7240-7251.

Lim LS, Chong G H, Tan PT, Chong Y-S, Kwek K, Gluckman PD, et al. Distribution and determinants of eye size and shape in newborn children: a magnetic resonance imaging analysis. Invest Ophthalmol Vis Sci 2013;54:4791-4797.

Lim LS, Yang X, Gazzard G, Lin X, Sng C, Saw SM, Qiu A. Variations in eye volume, surface area, and shape with refractive error in young children by magnetic resonance imaging analysis. Invest Ophthalmol Vis Sci 2011;52:8878-8883.

Shunmugam M, Shah AN, Hysi PG, Williamson TH. The pattern and distribution of retinal breaks in eyes with rhegmatogenous retinal detachment. Am J Ophthalmol 2014;157:221-226.

Mitry D, Singh J, Yorston D, Siddiqui MAR, Wright A, Fleck BW et al. The predisposing pathology and clinical characteristics in the Scottish retinal detachment study. Ophthalmology 2011;118:1429-1434.

Singh KD, Logan NS, Gilmartin B. Three-dimensional modeling of the human eye based on magnetic resonance imaging. Invest Ophthalmol Vis Sci 2006; 47:2272-2279.

Sheppard AL, Evans CJ, Singh KD, Wolffsohn JS, Dunne MC, Davies LN. Three-dimensional magnetic resonance imaging of the phakic crystalline lens during accommodation. Invest Ophthalmol Vis Sci 2011; 52:3689-3697.

Ogawa A, Tanaka M. The relationship between refractive errors and retinal detachment--analysis of 1,166 retinal detachment cases. Jpn J Ophthalmol 1987; 32.3:310-315.

Pierro L, Camesasca FI, Mischi M, Brancato R. Peripheral retinal changes and axial myopia. Retina 1992; 12.1:12-17.

Cheng SC, Lam CS, Yap MK. Prevalence of myopia-related retinal changes among 12–18 year old Hong Kong Chinese high myopes. Ophthalmic Physiol Opt 2013; 33:652-660.

TABLES

Table 1 Comparison of surface area data reported by previous studies

Study	Sample	Methods	Findings	Comments
Taylor and Jennings (1971)	N/A	Mathematical modelling based on schematic eyes	RSA and quadrant retinal surface areas for an emmetropic eye, with an axial length of 22.12mm, were estimated to be RSA 1133.8mm^2 IN 289.8mm^2 SN 286.8 mm^2 IT 280.4 mm^2 ST 276.8 mm^2	Calculations based on fixed values of axial length, corneal size, and the distance from ora serrata to limbus for each quadrant
Robb et al 1982	Children (n=33) Aged 6 months gestation to 6 years	Donor eye dissection	RSA: Range 300mm^2 to 907mm^2	Systemic conditions, which caused death, may have also impaired development of the eye (e.g. foetal anoxia)
Panda-Jonas et al 1994	Children and adults (n=46) Aged 2-90 years (mean age 50.7 ± 20.4 years)	Donor eye dissection	Mean RSA mean±sd: 1204±184 mm^2 Range 681-1636 mm^2	While there is a risk of tissue shrinkage, this was factored into the estimates of surface area.
Lim et al 2011	Children (n=67) Aged 6 years (mean age, 77.9±3.9 months) Participants were of Chinese ethnicity	In vivo 3-dimensional MRI	Mean TSA: 1757.05± 109.58 mm^2	3-Tesla scans. Did not investigate quadrant surface area
Lim et al 2013	Children (n=173) Aged 5-17 days Participants were of Chinese, Malay, and Indian ethnicity	In vivo 3-dimensional MRI	Mean TSA±sd: 898±70 mm^2 Range 677-1217 mm^2	1.5-Tesla scans. Did not investigate quadrant surface area
This study	Young-adults, aged 18-40 years.	In vivo 3-dimensional MRI	Mean TSA±sd: 2058±189 mm^2 Range	3-Tesla scans. Quadrant surface areas also reported

	Ethnicity predominantly White European (n=56%) and South Asian (n=38%)		1504 - 2716 mm^2 Mean RSA: 1363±160mm^2 Range 962-1857mm^2	

Table 2 Mean (RE) group data for MSE, AL, TSA, and mean QRSA ± 1 standard deviation.

Mean MSE (D)	**-2.50±4.03 (range -10.56 to +9.50)**
Mean PCI axial length (mm)	**24.51±1.57 (range 20.32-28.12)**
Mean TSA (mm^2)	**2058±189 (range 1504 to 2716)**
QRSAs (mm^2):	
Superior-temporal	**365±43**
Inferior-temporal	**340±40**
Superior-nasal	**337±40**
Inferior-nasal	**321±39**

Table 3 Differences between the internal MRI surface area and surface area for an equivalent sphere.

PCI axial length (mm)	Sphere TSA (mm^2)	MRI TSA (mm^2)	Difference (MRI-Sphere) (mm^2)	Percentage difference
22	1520	1809	289	15.98%
23	1661	1903	242	12.72%
24	1809	2001	192	9.60%
25	1963	2102	139	6.61%
26	2123	2207	84	3.81%
27	2289	2316	27	1.17%
27.50	2375	2371	-3	-0.17%
28	2462	2428	-34	-1.40%

TITLES AND LEGENDS TO FIGURES:

Figure 1 A) Correlation between MSE and Total Surface Area (TSA) B) Correlation between PCI Axial Length and Total Surface Area (TSA). C) Correlation between MSE and total retinal surface area (RSA). D) Correlation between PCI Axial Length and total retinal surface area (RSA). Data for REs.

Figure 2 MRI total internal surface area (TSA) and equivalent sphere surface area (r=PCI AL/2) both plotted as a function of PCI axial length. Data for REs.

Figure 3 Quadrant retinal surface area (QRSA) for the whole group plotted as a function of (A) PCI axial length and (B) MSE. Data for REs.

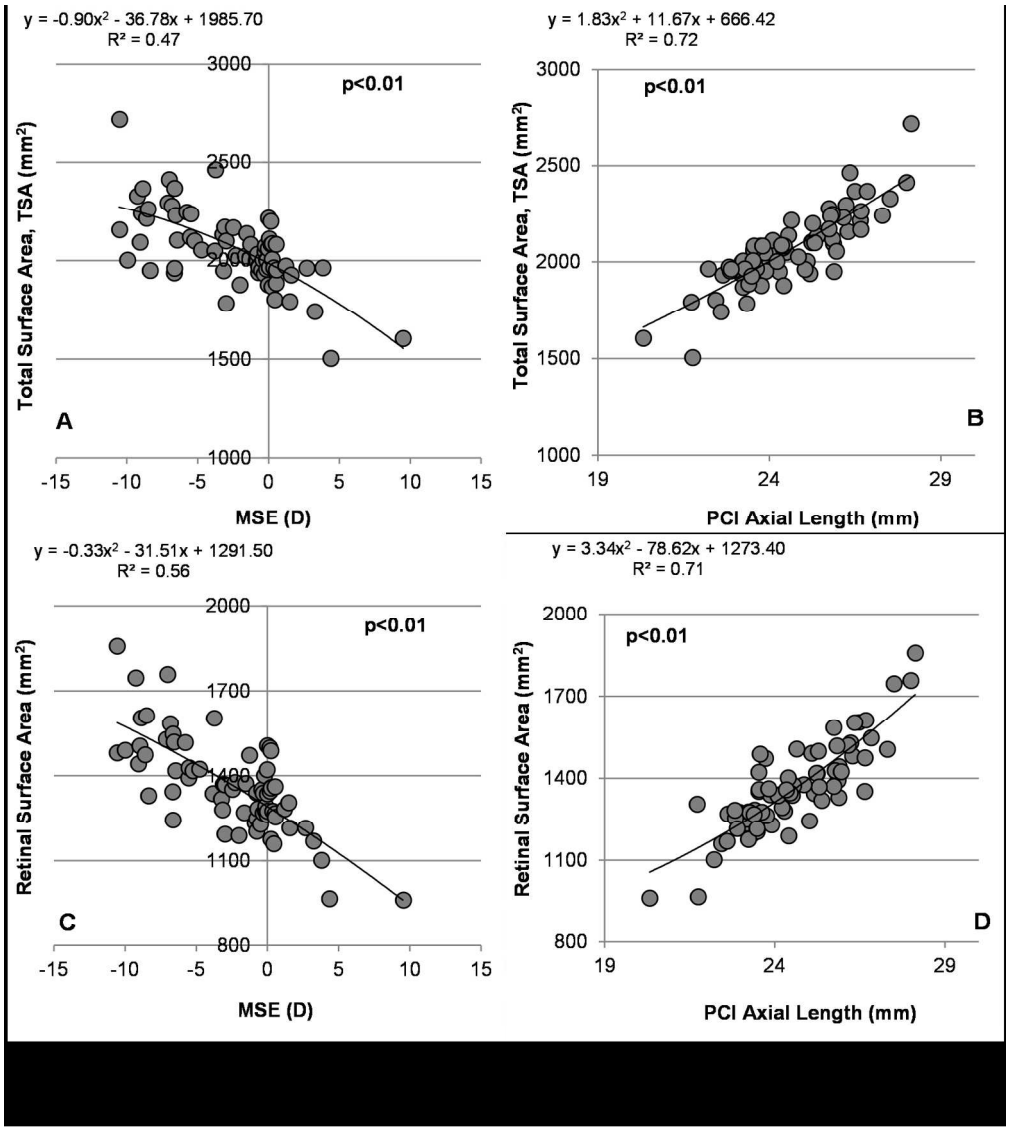

Figure 1 A) Correlation between MSE and Total Surface Area (TSA) B) Correlation between PCI Axial Length and Total Surface Area (TSA). C) Correlation between MSE and total retinal surface area (RSA). D) Correlation between PCI Axial Length and total retinal surface area (RSA). Data for REs.

159x178mm (300 x 300 DPI)

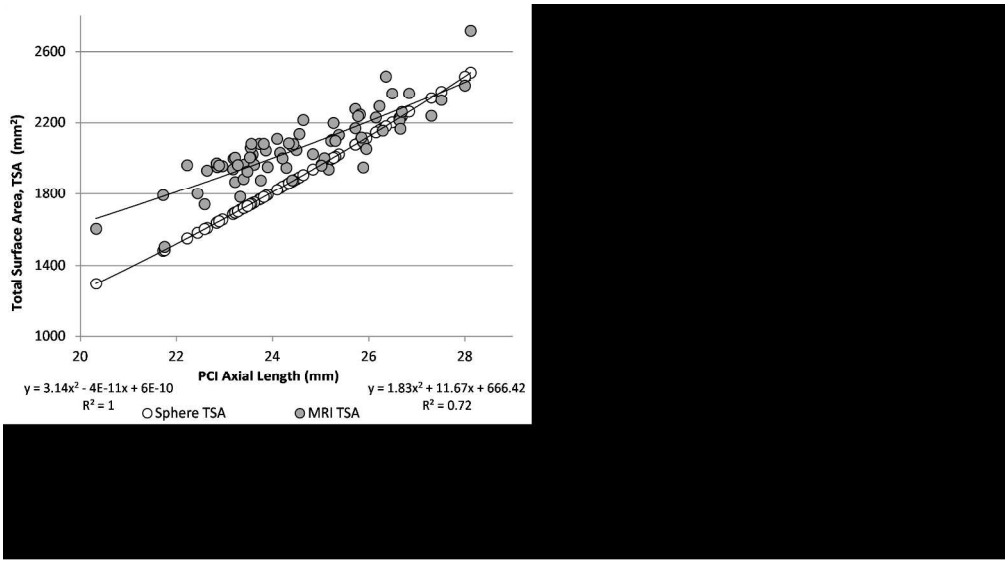

Figure 2 MRI total internal surface area (TSA) and equivalent sphere surface area (r=PCI AL/2) both plotted as a function of PCI axial length. Data for REs.

228x126mm (300 x 300 DPI)

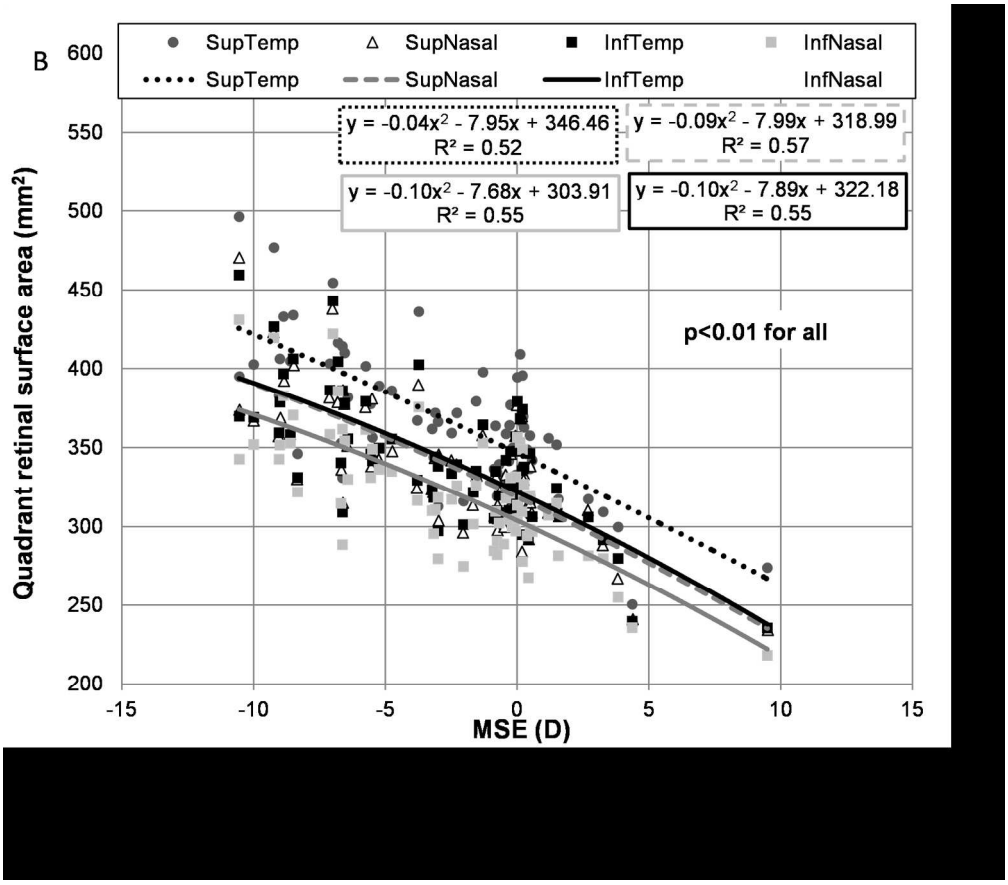

Figure 3 Quadrant retinal surface area (QRSA) for the whole group plotted as a function of (A) PCI axial length and (B) MSE. Data for REs.

165x144mm (300 x 300 DPI)